Frontiers in Bioscience Landmark

Front. Biosci. (Landmark Ed) **2026**; 31(2): 47070
https://doi.org/10.31083/FBL47070

Original Research

Inter-laboratory Evaluation of γH2AX/53BP1 DNA Double-strand Break Foci Assays in Human Lymphocytes Under Low-dose Irradiation: Implications for Calyculin A

Lucián Zastko[1,2,*,†], Lukáš Jakl[1,†], Jana Kružliaková[1], Petra Petrovičová[1]

[1]Department of Radiobiology, Cancer Research Institute, Biomedical Research Center, Slovak Academy of Sciences, 845 05 Bratislava, Slovakia
[2]Department of Laboratory Medicine, Faculty of Health Sciences, Catholic University in Ružomberok, 034 01 Ružomberok, Slovakia
*Correspondence: exonzast@savba.sk; lucian.zastko@ku.sk (Lucián Zastko)
[†]These authors contributed equally.

Academic Editor: Alexandros G. Georgakilas
Submitted: 30 September 2025 Revised: 16 January 2026 Accepted: 26 January 2026 Published: 24 February 2026

Abstract

Background: Accurate biodosimetry is essential for effective radiological triage, precise clinical monitoring, and assessment of risks from diagnostic exposures. Immunofluorescent detection of phosphorylated histone H2AX (γH2AX) and p53-binding protein 1 (53BP1) DNA double-strand break repair foci provides high sensitivity for radiation dose assessment within the first hours after exposure. However, inter-laboratory reproducibility of γH2AX/53BP1-based biodosimetry remains limited, and the contribution of pharmacological modifiers is unresolved. **Methods**: Here, we conducted an inter-laboratory comparison of *in vitro* radiation dose–response relationships of foci yields measured in cryopreserved umbilical cord blood lymphocytes (UCBLs) and freshly isolated peripheral blood lymphocytes (PBLs) from healthy donors using fluorescent microscopy with emphasis on workflow harmonization and reproducibility across laboratories. **Results**: Under low-dose γ irradiation, both UCBLs and PBLs exhibited a strong linear, dose-dependent induction of γH2AX, 53BP1, and co-localized foci, with co-localization emerging as the most sensitive endpoint. γH2AX pan-nuclear staining was observed exclusively in UCBLs and functioned as a distinct endpoint under the examined conditions. Under harmonized low-dose conditions, calyculin A at a non-toxic concentration of 1 nM did not provide measurable stabilization or enhancement of ionizing radiation-induced foci (IRIF) yields. Although IRIF yields differed between the two laboratories, dose–response slopes were highly concordant, demonstrating reproducibility under harmonized experimental conditions. **Conclusions**: These findings demonstrate that inter-laboratory reproducibility of γH2AX/53BP1-based biodosimetry is achieved primarily through disciplined workflow harmonization rather than through pharmacological enhancement. By reinforcing assay reproducibility and biological consistency, this work supports the translational applicability of IRIF-based biodosimetry for broader application in radiation exposure assessment.

Keywords: DNA double-strand breaks; DNA damage response; H2AX histone; 53BP1 protein; calyculin A; biodosimetry; lymphocytes; phosphatase inhibitors; ionizing radiation; immunofluorescence

1. Introduction

Accidental or deliberate exposure to ionizing radiation (IR) remains a serious public health concern, particularly in the context of nuclear accidents, radiological emergencies, and increasing geopolitical instability. Consequently, rapid, sensitive, and reliable biodosimetric tools are indispensable for population triage following radiological events [1]. Beyond emergency response, biodosimetry is increasingly applied in clinical practice, for example, for individualization of radiotherapy and monitoring of patient responses to IR [2,3]. In addition, sensitive biodosimetric approaches are required for the detection and evaluation of low-dose radiation exposures originating from diagnostic imaging procedures, including conventional X-rays [4,5], computed tomography [6,7], nuclear medicine [8–10], and other radiological examinations [11–16].

Among currently available assays, immunofluorescent detection of DNA double-strand break (DSB) repair foci, particularly those marked by phosphorylated histone H2AX (γH2AX) and p53-binding protein 1 (53BP1), represents one of the most sensitive approaches for assessing radiation-induced DNA damage at the single-cell level. These assays exhibit linear dose-response relationships even at low radiation doses, making them attractive candidates for biodosimetric applications [17–22]. However, despite their analytical sensitivity, several challenges limit their broader implementation, including inter-laboratory variability, rapid dephosphorylation of γH2AX leading to signal loss over time, and interference from apoptotic γH2AX pan-nuclear staining that can confound interpretation by mimicking DNA DSB-induced foci [23–27]. Consequently, the principal limitation for the broader deployment of γH2AX/53BP1-based biodosimetry is no longer sensitivity *per se*, but the lack of systematic validation of assay reproducibility under harmonized low-dose protocols.

In an effort to overcome these limitations, pharmacological modulation of DNA damage signaling pathways

has been explored [28]. Among several phosphatase inhibitors, including fostriecin and okadaic acid, calyculin A (cal A) has attracted particular attention. Cal A is a potent inhibitor of serine/threonine protein phosphatases 1 and 2A (PP1/PP2A) [29,30] and has been reported to stabilize γH2AX foci by inhibiting dephosphorylation events [31,32]. Originally described as a strong inducer of premature chromosome condensation in peripheral blood lymphocytes (PBL) [33], cal A has subsequently been proposed as a modifier of γH2AX signaling, although reported effects vary substantially across experimental workflows. Indeed, several studies reported prolonged persistence of γH2AX foci following irradiation in the presence of cal A, facilitating dose estimation particularly in the low-dose range [31,34]. Nevertheless, the reported effects of cal A remain highly context-dependent, complicating its routine use in biodosimetric applications [25,35,36]. Such discrepancies may reflect differences in experimental conditions, including cell type, cryopreservation protocols, irradiation settings, and subtle methodological variations.

Beyond practical biodosimetric implications, cal A interferes with fundamental DNA damage response mechanisms. Through inhibition of serine/threonine phosphatases, cal A can alter chromatin-associated signaling pathways, complicating the interpretation of radiation-induced foci (IRIF)-based readouts. In particular, apoptosis-associated γH2AX pan-staining, a recognized marker of early apoptotic processes [37,38], can obscure or mimic genuine IRIF, complicating accurate DSB quantification. Moreover, distinct lymphocyte subsets such as umbilical cord blood lymphocytes (UCBL), hematopoietic stem cells, and PBL, differ in their DNA damage responses and sensitivity to apoptosis, further challenging reproducibility across studies [23,36]. In this context, cal A is not considered here as an optimization strategy, but rather as a deliberate stress test to probe the biological consistency and robustness of γH2AX/53BP1 foci assays under harmonized experimental conditions.

Our previous work directly examined the effects of cal A on γH2AX/53BP1 foci formation in UCBL exposed to low and therapeutic doses *in vitro* [36]. That study demonstrated no stabilizing effect at either 1 or 10 nM cal A, while the higher concentration induced pronounced cytotoxicity and apoptotic signaling. Building on these findings, the present study was designed as an inter-laboratory evaluation of γH2AX/53BP1-based IRIF assays under harmonized low-dose workflows, using cal A as a test case to assess whether pharmacological modulation improves reproducibility. UCBL samples from a single provider were analyzed independently in two laboratories using identical cell processing, handling, irradiation protocols and cal A from the same supplier, with foci kinetics followed for up to 2 h post-irradiation. To address potential artifacts introduced by cryopreservation, analyses were extended in one laboratory to freshly isolated PBL, in which IRIF kinetics were examined for up to 6 h after irradiation. The study focused primarily on biologically and clinically relevant low-dose ranges, with higher doses included in PBL to explore dose-dependent effects under conditions free of cryopreservation stress. Cal A was restricted to a non-toxic concentration of 1 nM to assess whether foci stabilization could be achieved without compromising cellular viability. By focusing on inter-laboratory reproducibility under fully harmonized low-dose workflows, this work directly addresses a critical barrier to the standardization and translational readiness of γH2AX/53BP1-based biodosimetry.

2. Materials and Methods

All experimental procedures were designed to ensure maximal reproducibility between laboratories. Wherever possible, identical reagents, suppliers, incubation times, irradiation conditions, and image acquisition parameters were used. Methodological details are provided to explicitly document harmonization steps critical for inter-laboratory comparison rather than to serve as a procedural manual.

2.1 Chemicals

Reagent grade chemicals were obtained from Sigma-Aldrich (St. Louis, MO, USA), Merck KGaA (Darmstadt, Germany) and Life Technologies (Carlsbad, CA, USA). Cal A was purchased from Abcam Biochemicals (Cambridge, UK) and dissolved in dimethyl sulfoxide (DMSO; SERVA Electrophoresis GmbH, Heidelberg, Germany).

2.2 Cells

UCB mononuclear cells (MNC) were extracted as previously described [27] from 3 healthy newborns after full-term pregnancies and provided by Eurocord-Slovakia, Bratislava, Slovakia. In Laboratory 1, cryopreserved UCB MNC from three donors were thawed using standard protocols and cultured in RPMI 1640-based basal medium supplemented with fetal bovine serum and antibiotics. Monocytes were removed by short-term adherence.

In Laboratory 2, UCB MNC from three independent donors obtained under identical inclusion criteria were analyzed as part of a previously published dataset [36] and used here exclusively for inter-laboratory comparison at matched irradiation doses and time points. Except for fixation timing, identical cell handling and processing steps were applied in both laboratories.

Peripheral blood (PB) MNC were isolated from six healthy adult donors by density-gradient centrifugation as previously described [39]. Monocytes were removed by adherence, yielding predominantly lymphocyte populations. Cell viability exceeded 95% in all experiments as assessed by Trypan blue exclusion.

Cell Authenticity and Quality Control

All experiments were performed using primary human mononuclear cells isolated directly from umbilical cord blood or peripheral blood of healthy donors. These cells were not cultured or passaged and were used immediately after isolation (PBL) or after standardized cryopreservation and thawing (UCBL). Cell identity was ensured by established lymphocyte isolation procedures, donor documentation, and ethical approval. Cell morphology was examined by light microscopy, and cell viability exceeded 95% as assessed by trypan blue exclusion. As the study did not involve immortalized cell lines or long-term cell culture, STR profiling and routine mycoplasma testing were not applicable.

2.3 Cell Treatment

Following equilibration, lymphocytes were divided into three treatment groups: cal A (1 nM), DMSO vehicle control (0.1%), and untreated controls. Cells were incubated on ice for approximately 40 min prior to irradiation to synchronize handling between laboratories. To avoid prolonged exposure-related toxicity, cal A and DMSO were added immediately after irradiation in both laboratories, consistent with our previous observations [36].

2.4 Irradiation

Cells were irradiated on ice using acute γ-rays at a dose rate of approximately 45 cGy/min. UCBL were exposed to doses of 10, 50, 100, 500, and 1000 mGy, while PBL were irradiated at 10, 100, and 1000 mGy. Irradiations were performed using ^{60}Co sources (Theratron Elite 100, MDS Nordion, Canada; or TERAGAM® K-02, UJP Praha, Czech Republic). Dose deviations did not exceed 5%. After irradiation, cells were rapidly warmed to 37 °C and incubated under standard culture conditions until fixation.

2.5 Immunofluorescence and Image Acquisition

At defined time points post-irradiation (0.5, 1, and 2 h for UCBL; 2, 4, and 6 h for PBL), cells were cytocentrifuged onto poly-L-lysine-coated slides, fixed with paraformaldehyde, permeabilized, and blocked according to standard protocols. γH2AX and 53BP1 were detected using well-characterized primary antibodies provided by Novus Biologicals, Abingdon, UK - monoclonal γH2AX anti-mouse (1:800, NB100-78356) and polyclonal 53BP1 anti-rabbit (1:1000, NB100-304); followed by Alexa Fluor-conjugated secondary antibodies (Invitrogen Molecular Probes, Life Technologies, OR, USA) - 488 IgG (H+L) polyclonal anti-rabbit (1:200, A11029) and 555 IgG (H+L) monoclonal anti-mouse (1:200, 21429). Nuclei were counterstained with DAPI-containing antifade medium.

Image acquisition was performed in both laboratories using Metafer Slide Scanning Systems V 3.9 (MetaSystems GmbH, Altlussheim, Germany) coupled to Zeiss Axio Imager fluorescence microscopes (Carl Zeiss Microscopy GmbH, Gottingen, Germany) under identical acquisition settings. For each condition, at least 600 cells were analyzed. Automated scoring of γH2AX and 53BP1 foci was conducted as previously described [16,40] and verified by manual inspection. Co-localized foci were defined by spatial overlap within 0.5 µm. γH2AX pan-nuclear staining was quantified in UCBL as an apoptosis-associated endpoint but was not observed in PBL.

2.6 Statistical Analysis

The yields of foci (Y) were expressed per cell. At each experimental dose point in cells of each blood donor the foci-per-cell distribution was checked for compliance with the Poisson model by χ^2 test. When individual data were pooled, standard errors (SE), standard deviations (SD) or $\pm$0.95 confidence intervals (CI) for the mean foci yield were calculated from the dispersion of donors' individual values within the group. The group data were analyzed using factorial analysis of variance (ANOVA) together with control for the false discovery rate (FDR). For pooled datasets fitting a normal distribution and involving a single categorical independent variable, comparisons between groups were performed by one-way ANOVA, followed by Fisher's LSD *post hoc* test. Associations between groups were assessed using the Spearman rank-order correlation test (ROC), while correlations between independent groups were evaluated with the Mann-Whitney U test. These statistical analyses were performed with Statistica 8.0 software (StatSoft Inc., Tulsa, OK, USA). Differences were considered statistically significant at $p < 0.05$.

Dose-response relationships for the foci yield were fitted by the iteratively reweighted least squares method to the linear model:

$$Y = c + \alpha \times D,$$

where Y - foci yield per cell; c - the background foci level; α - linear coefficient representing a foci induction rate per unit dose; D - radiation dose in Gy. Goodness of fit was assessed by a linear correlation coefficient (r). The coefficient α was compared between blood donors or laboratories as normally distributed parameter, using the unpaired Student's t-test. The statistical software package Dose Estimate_v.5.1 [41] was used to perform foci distribution testing and dose-response curve fitting; the latter was carried out assuming Poisson foci-per-cell distribution for calculations of coefficient errors.

3. Results

3.1 Dose-response Characteristics and Assay Sensitivity in UCBL Across Laboratories

For each UCBL donor, the foci-per-cell distributions in unirradiated and irradiated samples were consistent with

Table 1. Coefficients of the dose-response regressions.

End-point	Laboratory 1			Laboratory 2		
	$c \pm$ SE	$\alpha \pm$ SE	r	$c \pm$ SE	$\alpha \pm$ SE	r
γH2AX	0.4199 $\pm$ 0.0937	7.2150 $\pm$ 0.3257	0.9976	0.7105 $\pm$ 0.1443	7.4690 $\pm$ 0.6067	0.9987
53BP1	0.2436 $\pm$ 0.3054	7.6600 $\pm$ 1.2410	0.9491	1.0829 $\pm$ 0.1749	5.1370 $\pm$ 0.6155	0.9951
γH2AX/53BP1	0.2021 $\pm$ 0.1773	6.0960 $\pm$ 0.7121	0.9778	0.3081 $\pm$ 0.1289	4.2980 $\pm$ 0.5776	0.9958

Values represent coefficients of the linear dose-response model $Y = c\ (\pm\ \text{SE}) + \alpha\ (\pm\ \text{SE}) \times D$, where Y is the foci yield per cell, c is foci spontaneous (control) level, α is foci induction rate per unit dose, D is radiation dose in Gy, SE is standard error; r is linear correlation coefficient. Curve fitting was carried out with pooling individual data from cells of three donors in Laboratory 1 and three other donors in Laboratory 2. SE were estimated assuming Poisson distribution of foci among cells. γH2AX, phosphorylated histone H2AX; 53BP1, p53-binding protein 1.

Poisson statistics, as expected for homogeneous exposure to low-LET radiation (data not shown). Donor-specific regression coefficients are summarized in **Supplementary Table 1**, and pooled regressions for each laboratory are shown in Table 1 and Fig. 1.

Across both laboratories, γH2AX, 53BP1, and γH2AX/53BP1 co-localized foci displayed strong linear dose-response relationships within the investigated dose range, with excellent goodness-of-fit to the linear model ($r \geq 0.94$ for all endpoints; Table 1). In Laboratory 1 (UCBL fixed 0.5 h post-irradiation), all three endpoints were significantly elevated already at 50 mGy relative to unirradiated controls, indicating early sensitivity above endogenous foci levels. In Laboratory 2 (UCBL fixed 2 h post-irradiation), co-localized foci remained the most sensitive endpoint (significant induction at 50 mGy), while separate γH2AX and 53BP1 foci reached statistical significance at 100 mGy. This time-dependent shift in the apparent sensitivity pattern is consistent with the known differences in foci kinetics during the first post-exposure hours.

Importantly, because the two laboratories quantified foci at different post-irradiation times (0.5 h vs 2 h), absolute foci yields between laboratories are not interpreted as direct head-to-head "inter-laboratory disagreement". Instead, the inter-laboratory comparison is focused on (i) the reproducibility of the dose-response form (linearity), (ii) the similarity of regression slopes (α), and (iii) the consistency of conclusions regarding cal A effects under harmonized processing and scoring workflows. In this context, pooled regression analysis indicated highly comparable γH2AX induction rates per unit dose between laboratories, whereas α values for 53BP1 and co-localized foci were numerically lower in Laboratory 2; these differences did not reach statistical significance (Table 1). Overall, the narrow range of α values supports reproducible dose-response relationships despite differences in fixation time and donor sets.

Together, these results establish that the γH2AX/53BP1 IRIF assay provides robust, quantitative, and highly sensitive detection of radiation-induced DNA damage in UCBL within the low-dose range, and that dose-response relationships remain reproducible across independent laboratories when protocols are workflow-aligned and key steps are harmonized.

3.2 UCBL: Effects of Dose, Treatment, and Post-irradiation Time in Laboratory 1

Laboratory 1 assessed the effects of irradiation dose (0, 10, 50, 100 mGy), treatment condition (cal A, DMSO vehicle, untreated), and post-irradiation time (0.5, 1, 2 h) on γH2AX, 53BP1, and co-localized foci, as well as on the frequency of γH2AX pan-nuclear staining in UCBL (Table 2). Multivariate ANOVA identified irradiation dose as the only significant factor across foci endpoints. Treatment condition and time within the first 2 h did not reach statistical significance, indicating that foci levels were primarily determined by dose under the applied experimental conditions.

Univariate testing confirmed a highly significant dose dependence for γH2AX, 53BP1, and co-localized foci (all FDR-adjusted $p < 0.00001$; Table 2). In contrast, neither treatment (cal A or DMSO) nor post-irradiation time significantly altered foci yields. γH2AX pan-staining showed no significant dependence on dose, treatment, or time within this experimental window (Table 2), supporting its interpretation as a distinct endpoint not tracking with repair foci formation under low-dose conditions.

Vehicle Control and Cal A Effect in Laboratory 1

Untreated UCBL were compared with matched DMSO-treated samples at identical doses and time points. No significant differences were detected, validating DMSO as an appropriate vehicle control. For clarity, untreated data were omitted from Fig. 2, which focuses on direct cal A vs DMSO comparisons. As shown in Fig. 2, foci yields are presented across multiple doses, time points, and treatments to illustrate overall assay behavior under the experimental design; no direct quantitative comparison between post-irradiation time points is intended.

As shown in Fig. 2, γH2AX, 53BP1, and co-localized foci increased with irradiation dose at all time points (0.5, 1, 2 h). Critically, cal A at 1 nM did not produce a systematic increase in foci yield or altered kinetics relative to DMSO controls at any dose or time point examined. γH2AX pan-staining remained low and comparable between treatments.

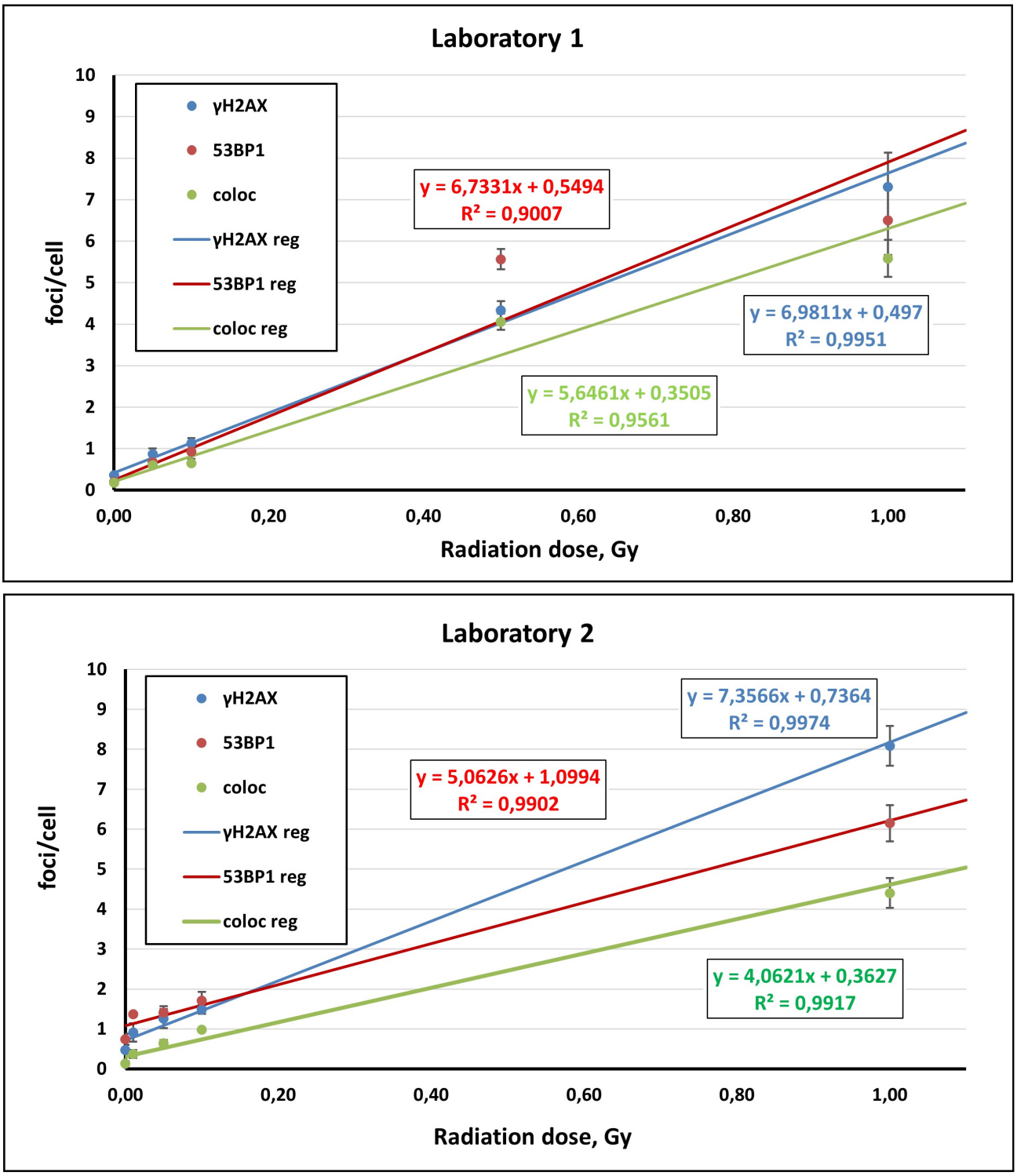

Fig. 1. Linear dose-response relationships for γH2AX, 53BP1, and γH2AX/53BP1 co-localized foci in umbilical cord blood lymphocytes (UCBL). Mean foci yields per cell (± SE) are shown as a function of γ-irradiation dose for Laboratory 1 (cells fixed 0.5 h post-irradiation) and Laboratory 2 (cells fixed 2 h post-irradiation). Solid lines represent linear regressions fitted according to $Y = c + \alpha \times D$, with corresponding regression equations and coefficients of determination (R^2) displayed in each panel. Regression coefficients (α) and correlation parameters are summarized in Table 1 and **Supplementary Table 1**. Differences in absolute foci yields between laboratories reflect distinct post-irradiation fixation times and donor sets and are not interpreted as direct inter-laboratory discrepancies. In all the data, the comma is used as the decimal separator. γH2AX, phosphorylated histone H2AX; 53BP1, p53-binding protein 1.

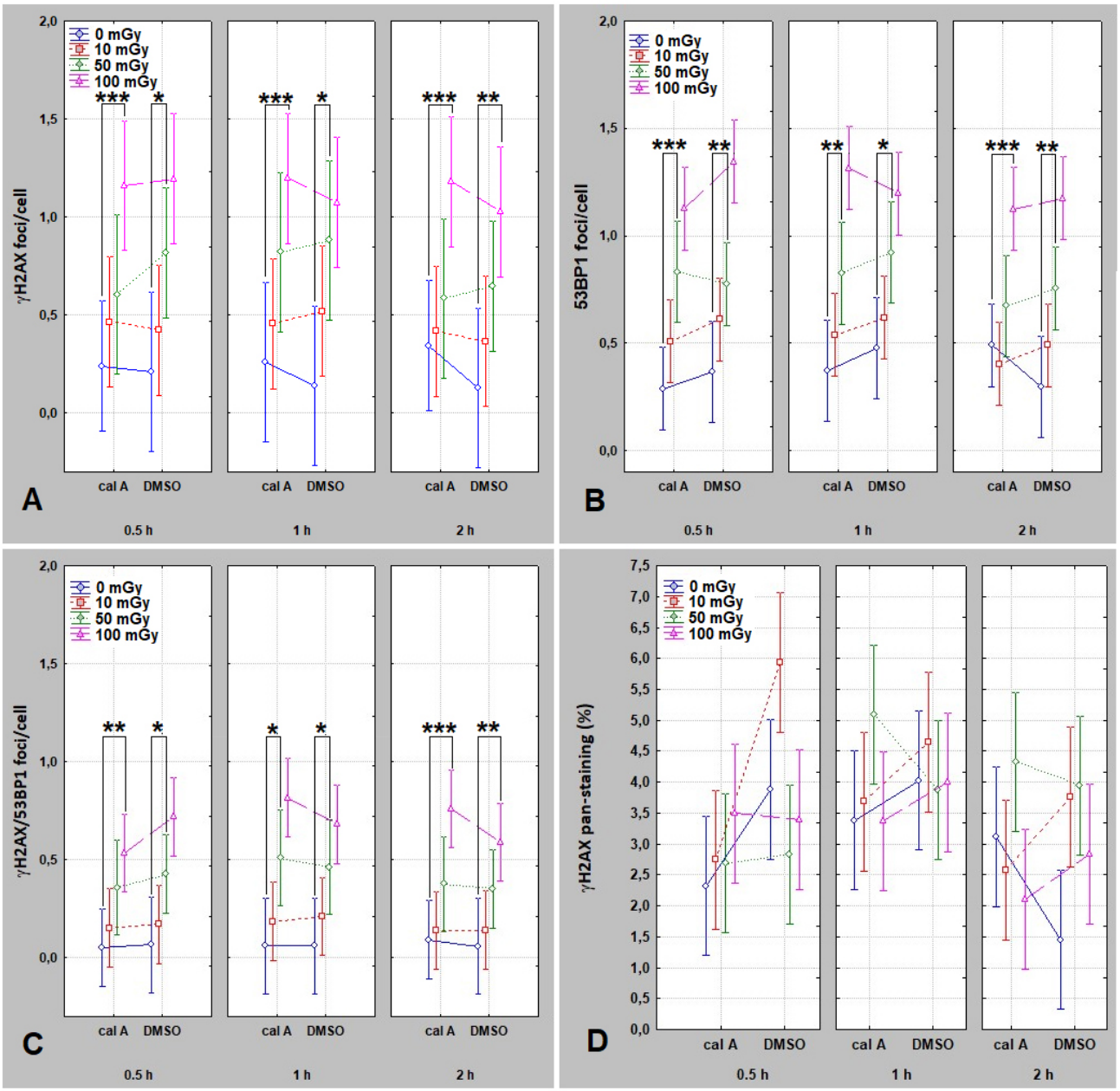

Fig. 2. Dose- and time-dependent induction of DNA repair foci in UCBL treated with DMSO or cal A - Laboratory 1. Panels show mean ±0.95 confidence interval from 3 experiments for (A) γH2AX foci per cell, (B) 53BP1 foci per cell, (C) co-localized γH2AX/53BP1 foci per cell, and (D) percentage of γH2AX pan-stained cells. For each endpoint, cells were irradiated with 0, 10, 50, and 100 mGy and analyzed at 0.5, 1, and 2 h post-irradiation/treatment. Concentrations - DMSO (0.1%) and cal A (1 nM). A minimum of 600 nuclei per condition was evaluated. Asterisks indicate significance versus the unirradiated control (0 mGy) within the same treatment group (DMSO or cal A) as determined by Fisher's LSD *post hoc* testing: * $p < 0.05$, ** $p < 0.01$, *** $p < 0.001$ (statistical procedures as described in Methods). Note: the figure illustrates the multivariate experimental design (dose × time × treatment) and endpoint behavior across conditions. It is intended to visualize qualitative trends and experimental structure rather than to enable direct quantitative comparison between different post-irradiation time points. In all the data, the comma is used as the decimal separator.

Table 2. Statistical testing dependence of DNA repair foci means and portion of γH2AX pan-stained UCBL on categorical factors.

Variables				Factorial ANOVA		Categorical factors			*p*-values adjusted by FDR		
γH2AX *	53BP1 *	γH2AX/53BP1 *	γH2AX pan-st. (%)	Multivariate	Univariate	Dose	Treatment	Post-irradiation Time	Dose	Treatment	Post-irradiation Time
+	+	+	+	+	–	+	+	+	0.00000	0.38884	0.20207
+	–	–	–	–	+	+	+	+	0.00000	0.72719	0.65372
–	+	–	–	–	+	+	+	+	0.00000	0.29701	0.13051
–	–	+	–	–	+	+	+	+	0.00000	0.84937	0.43122
–	–	–	+	–	+	+	+	+	0.59673	0.40271	0.33894

Categorical factors: radiation dose (Dose), cal A/DMSO treatments (Treatment), and post-irradiation time (0.5, 1, and 2 h). Where applicable, multivariate (across foci endpoints) and univariate tests are shown. Reported *p*-values are FDR-adjusted. * mean, foci per cell; + the data were included in analysis; – data were not included in analysis. Statistically significant values are marked in red. UCBL, umbilical cord blood lymphocytes; FDR, false discovery rate.

Table 3. Statistical testing dependence of DNA repair foci means and portion of γH2AX pan-stained UCBL 2 h post-irradiation/treatment on categorical factors.

Variables				Factorial ANOVA		Categorical factors			*p*-values adjusted by FDR		
γH2AX *	53BP1 *	γH2AX/53BP1 *	γH2AX pan-st. (%)	Multivariate	Univariate	Laboratory	Treatment	Dose	Laboratory	Treatment	Dose
+	+	+	+	+	–	+	+	+	0.00000	0.32265	0.00000
+	–	–	–	–	+	+	+	+	0.00000	0.38422	0.00000
–	+	–	–	–	+	+	+	+	0.00000	0.93173	0.00000
–	–	+	–	–	+	+	+	+	0.00001	0.29985	0.00000
–	–	–	+	–	+	+	+	+	0.23427	0.07822	0.54648

Categorical factors: laboratory relevant (Laboratory), radiation dose (Dose), and cal A/DMSO treatments (Treatment). Where applicable, multivariate (across foci endpoints) and univariate tests are shown. Reported *p*-values are FDR-adjusted. * mean, foci per cell; + the data were included in analysis; – data were not included in analysis. Statistically significant values are marked in red. UCBL, umbilical cord blood lymphocytes; FDR, false discovery rate.

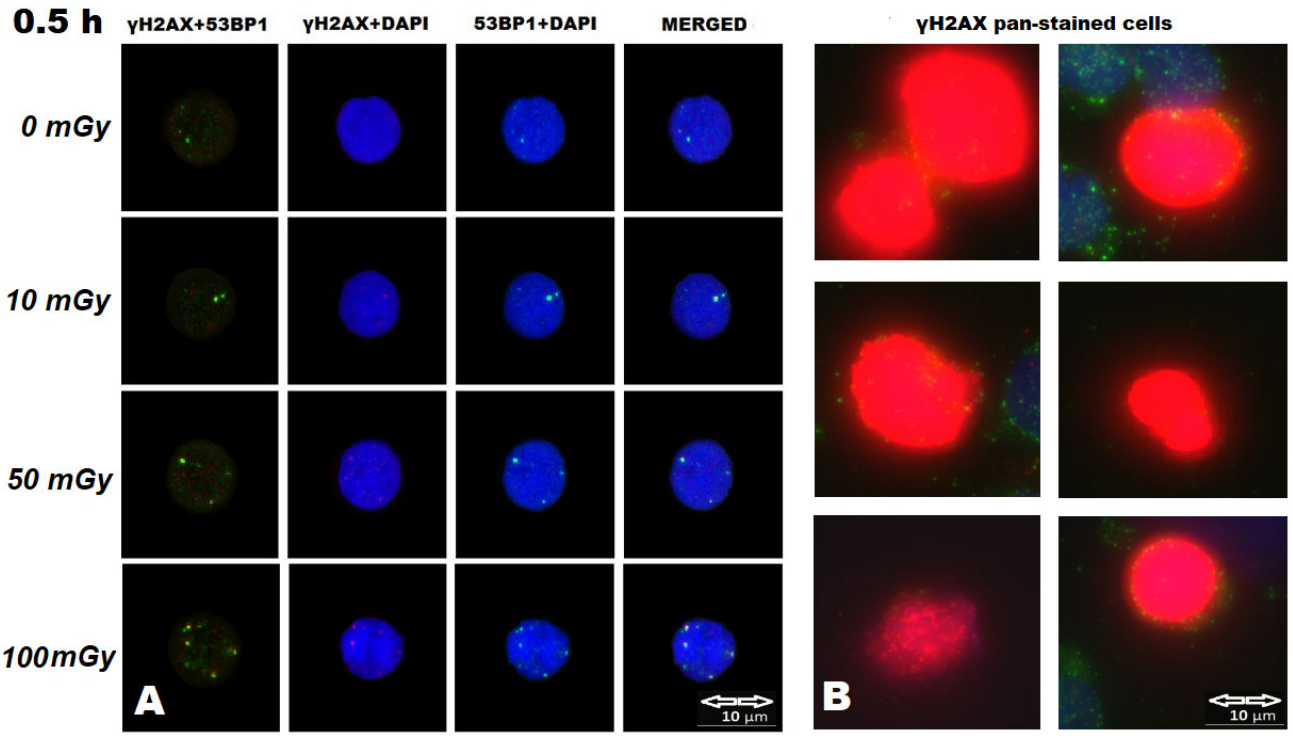

Fig. 3. Representative immunofluorescence images of UCBL nuclei analyzed for γH2AX/53BP1 foci, irradiated with 0, 10, 50, or 100 mGy and fixed at 0.5 h post-irradiation, followed by treatment with cal A (1 nM). Shown are examples of (A) nuclei exhibiting discrete γH2AX foci (red), 53BP1 foci (green), co-localized γH2AX/53BP1 foci (yellow), and (B) γH2AX pan-staining (diffuse nuclear red staining). Scale bar = 10 µm. Nuclei were counterstained with DAPI (blue). The images represent typical results from more than 600 cells scored per condition. Automated image acquisition was performed using the Metafer Slide Scanning System and Zeiss Axio Imager Z2 microscope under identical settings across all samples. These representative micrographs illustrate the main categories of DNA damage response endpoints evaluated quantitatively in Fig. 2.

Strong positive correlations were observed among γH2AX, 53BP1, and co-localized foci, whereas pan-staining did not correlate with foci-based endpoints, consistent with an apoptosis-associated signal distinct from DSB repair foci formation. Representative immunofluorescence images are provided in Fig. 3.

3.3 Inter-laboratory Comparison of UCBL at the Matched 2 h Time Point

To enable a time-matched inter-laboratory comparison, we evaluated UCBL data acquired at 2 h post-irradiation (Laboratory 1:2 h time point from the present study; Laboratory 2:2 h dataset reported previously and included here specifically for comparative evaluation). A three-way factorial ANOVA (Laboratory, Treatment, Dose) was performed (Table 3).

A significant laboratory factor was detected for γH2AX, 53BP1, and co-localized foci (all $p < 0.00001$), indicating systematic differences in absolute foci yields between laboratories. In contrast, no laboratory effect was observed for pan-staining ($p = 0.234$). The treatment factor (1 nM cal A vs 0.1% DMSO) was not significant for any foci endpoint (all $p > 0.3$). For pan-staining, the treatment effect showed a near-threshold trend ($p = 0.078$) that did not remain significant after correction, suggesting at most a weak influence under these conditions. Irradiation dose remained the dominant determinant of foci induction (all foci endpoints $p < 0.00001$ after FDR adjustment), while pan-staining again showed no dose dependence ($p = 0.546$).

Fig. 4 visualizes the 2 h comparison and confirms three core outcomes: (i) robust dose-dependent induction of γH2AX, 53BP1, and co-localized foci in both laboratories, (ii) systematic inter-laboratory offsets in absolute foci yields, and (iii) the absence of a detectable stabilizing effect of 1 nM cal A relative to DMSO. Correlation analyses supported high internal consistency among the three foci endpoints in each laboratory, while pan-staining remained uncorrelated. Non-parametric Mann-Whitney testing confirmed significant inter-laboratory differences in absolute foci counts for all three foci endpoints, but not for pan-staining.

Taken together, the time-matched comparison shows that while absolute yields can differ between laboratories, dose-response relationships and the qualitative treatment conclusion (no cal A stabilization at 1 nM) are reproducible under harmonized workflows.

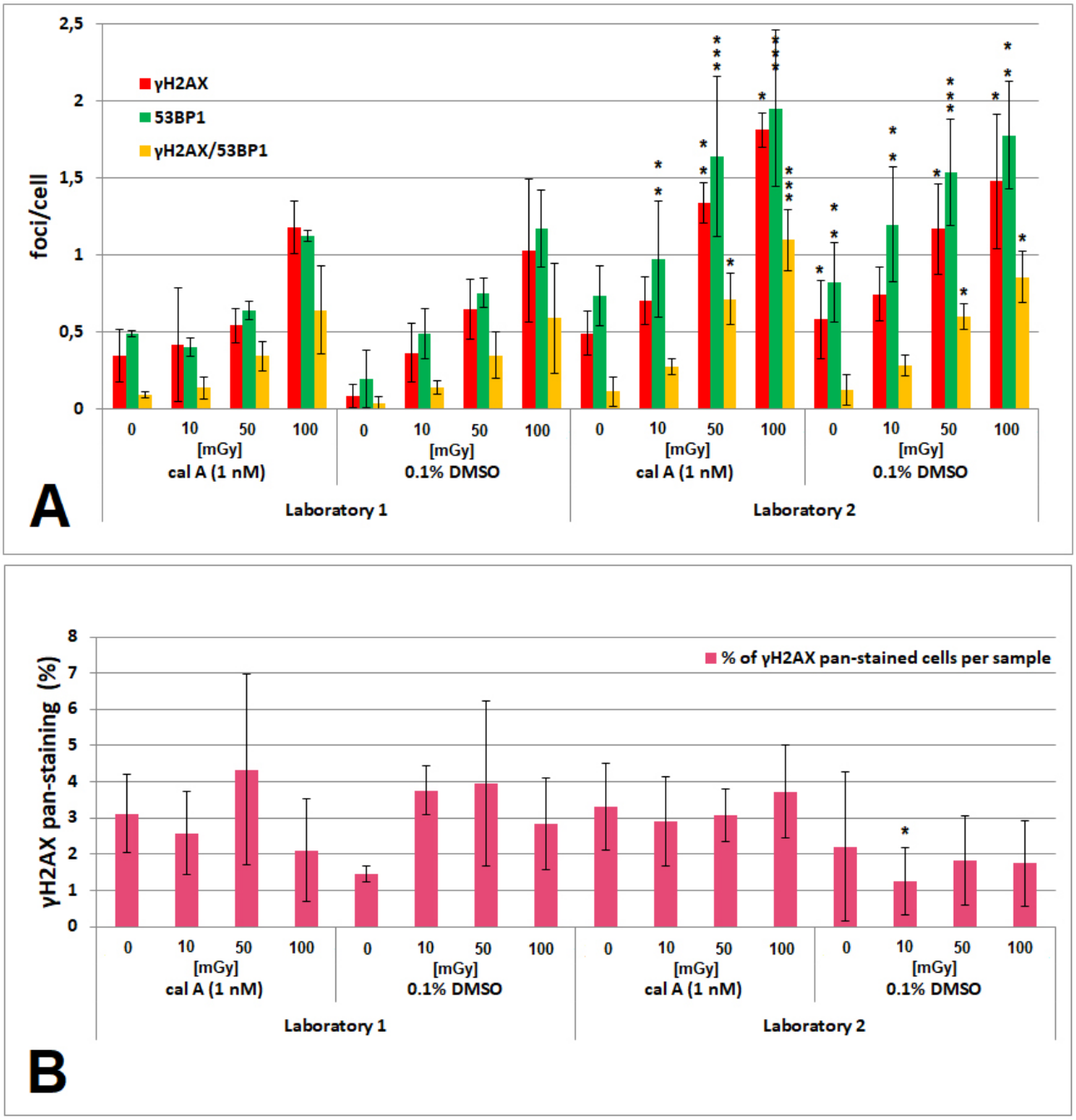

Fig. 4. Inter-laboratory comparison of γH2AX, 53BP1, co-localized γH2AX/53BP1 foci, and γH2AX pan-staining 2 h after low-dose γ-irradiation. (A) Mean ± SD foci per cell for γH2AX (red), 53BP1 (green), and γH2AX/53BP1 co-localized foci (yellow) at 0, 10, 50, and 100 mGy. (B) Mean ± SD percentage of γH2AX pan-stained nuclei under the same conditions. Data are shown separately for Laboratory 1 and Laboratory 2, each analyzing three independent donors. Cells were treated immediately after irradiation with either cal A (1 nM) or control (0.1% DMSO). At least 600 nuclei per condition were evaluated using automated image acquisition and scoring. Asterisks indicate statistically significant differences between Laboratory 1 and Laboratory 2 under identical irradiation and treatment conditions, as determined by Fisher's LSD *post hoc* testing: * $p < 0.05$, ** $p < 0.01$, *** $p < 0.001$. In all the data, the comma is used as the decimal separator.

3.4 PBL Responses to Dose, Treatment, and Time (Laboratory 2)

To assess whether findings in cryopreserved UCBL generalize to fresh adult lymphocytes and to reduce potential freeze-thaw confounding, peripheral blood lymphocytes (PBL) were analyzed in Laboratory 2 across doses and time points (Table 4; Fig. 5). Factorial ANOVA demonstrated highly significant dose effects for all foci endpoints

Table 4. Statistical testing dependence of DNA repair foci means in PBL on categorical factors.

Variables			Factorial ANOVA		Categorical Factors			*p*-values adjusted by FDR		
γH2AX *	53BP1 *	γH2AX/53BP1 *	Multivariate	Univariate	Dose	Treatment	Post-irradiation Time	Dose	Treatment	Post-irradiation Time
+	+	+	+	–	+	+	–	0.00000	0.12145	–
+	–	–	–	+	+	+	–	0.00000	0.64753	–
–	+	–	–	+	+	+	–	0.00000	0.26433	–
–	–	+	–	+	+	+	–	0.00000	0.08321	–
+	+	+	+	–	+	+	+	0.00040	0.40890	0.86156
+	–	–	–	+	+	+	+	0.00018	0.37226	0.87154
–	+	–	–	+	+	+	+	0.00461	0.97609	0.77227
–	–	+	–	+	+	+	+	0.00006	0.38582	0.47825

Factors included in the first 4 row-based cases - 0, 10, and 1000 mGy radiation dose (Dose) and cal A-, DMSO-, and non-treatments (Treatment) measured at 2 h post-irradiation/treatment; factors included in the last 4 row-based cases - 0 and 100 mGy radiation dose, cal A-, DMSO-, and non-treatments, and Post-irradiation Time (2, 4, and 6 h). Where applicable, multivariate (across foci endpoints) and univariate tests are shown. Reported *p*-values are FDR-adjusted. * mean, foci per cell; + the data were included in analysis; – data were not included in analysis. Statistically significant values are marked in red. PBL, peripheral blood lymphocytes; FDR, false discovery rate.

at 2 h (FDR-adjusted $p < 0.001$) and similarly when including extended time points (2, 4, 6 h) at 0 and 100 mGy (FDR-adjusted $p < 0.005$). Treatment and post-irradiation time did not significantly affect foci levels (FDR-adjusted $p > 0.3$ and $p > 0.4$, respectively).

Notably, γH2AX pan-nuclear staining was not detected in PBL under any tested condition, in contrast to UCBL where pan-staining was consistently measurable. This difference indicates that pan-staining is not an inherent feature of lymphocytes under low-dose irradiation but depends on cell system and/or pre-analytical handling such as cryopreservation.

Vehicle Control Validation and cal A Effect in PBL

Inclusion of untreated irradiated PBL alongside DMSO- and cal A-treated samples confirmed that DMSO did not alter foci induction compared with untreated controls, supporting its use as vehicle control (Fig. 5). At low doses (0, 10, 100 mGy) and across time points (2, 4, 6 h), cal A did not significantly modify foci induction relative to DMSO or untreated controls.

A significant treatment-dependent effect emerged only at the highest dose tested: at 1000 mGy, co-localized γH2AX/53BP1 foci were significantly reduced in cal A-treated samples compared with DMSO controls ($p < 0.0014$; Fig. 5). This observation indicates that phosphatase inhibition does not universally preserve repair foci and, under high-dose conditions, may be associated with reduced co-localization persistence.

3.5 Cell-type-specific Response Patterns: PBL Versus UCBL Across Laboratories

Under comparable experimental conditions, both UCBL (in both laboratories) and PBL exhibited dose-dependent induction of γH2AX, 53BP1, and co-localized foci. However, two consistent differences were observed. First, γH2AX pan-staining was present in UCBL but absent in PBL, suggesting that apoptotic γH2AX signaling is influenced by cell type and/or cryopreservation-related pre-analytical factors. Second, cal A at 1 nM did not produce stabilizing effects in either system across the low-dose range; the only statistically significant treatment-related effect was a reduction of co-localized foci in PBL at 1000 mGy.

Overall, these results support high robustness of IRIF dose-response relationships under harmonized workflows while indicating that the impact of cal A is strongly context-dependent and not reliably stabilizing under the tested conditions.

4. Discussion

4.1 Summary of Principal Findings

Across two independent laboratories, γH2AX, 53BP1, and γH2AX/53BP1 co-localized foci in UCBL showed reproducible linear dose-response relationships under harmonized low-dose workflows. γH2AX pan-nuclear staining represented a biologically distinct endpoint, uncoupled from dose-response behavior and repair foci formation under the examined low-dose conditions. Importantly, under harmonized low-dose conditions, cal A (1 nM) did not provide any measurable stabilization or enhancement of IRIF yields. Where data are shown across multiple post-irradiation times, comparisons are interpreted qualitatively and within each time point, rather than as direct kinetic analyses.

Although absolute IRIF yields differed between laboratories, the form and linearity of the dose-response relationships were preserved across endpoints. Crucially, the qualitative conclusion regarding cal A was consistent across laboratories. Although these findings confirm the expected low-dose sensitivity of γH2AX/53BP1 foci induc-

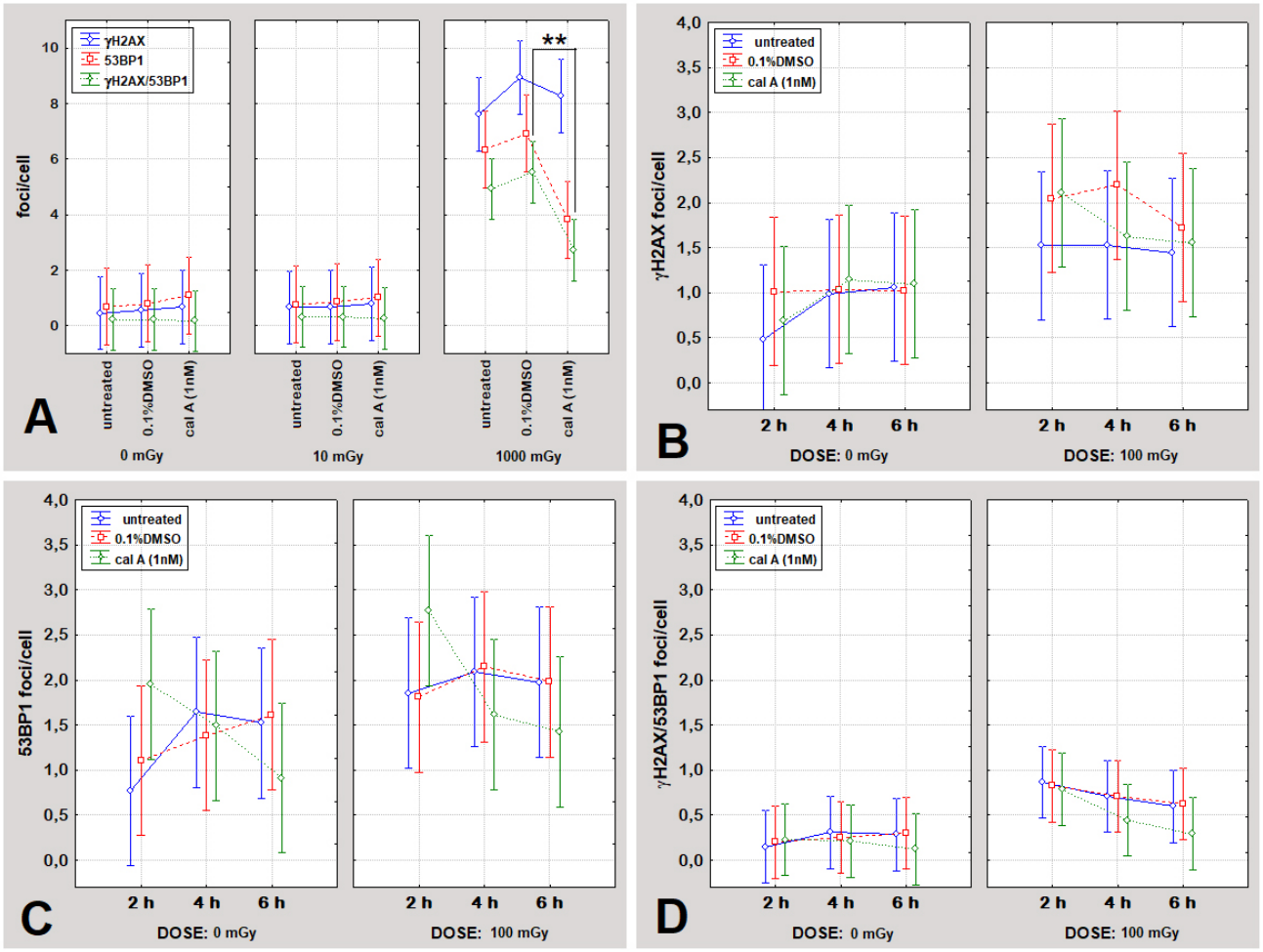

Fig. 5. Induction of DNA repair foci in PBL across treatments and irradiation conditions - Laboratory 2. (A) Mean numbers of γH2AX, 53BP1, and co-localized γH2AX/53BP1 foci per cell [±0.95 confidence interval (CI) from 3 experiments] are shown for untreated irradiated cells, DMSO-treated cells, and cal A (1 nM)-treated cells at 0, 10, and 1000 mGy, assessed 2 h post-irradiation/treatment. (B) Mean γH2AX foci per cell (±0.95 CI) at 0 and 100 mGy measured at 2, 4, and 6 h post-irradiation/treatment. (C) 53BP1 foci per cell (±0.95 CI) under the same conditions. (D) γH2AX/53BP1 co-localized foci per cell (±0.95 CI) under the same conditions. A significant reduction of γH2AX/53BP1 co-localization in-between treatments as determined by Fisher's LSD *post hoc* testing is indicated by ** $p <$ 0.01. A minimum of 600 nuclei were analyzed per condition using automated image acquisition and scoring. In all the data, the comma is used as the decimal separator.

tion, the principal contribution of this study lies in demonstrating that harmonized experimental workflows yield reproducible dose-response relationships across independent laboratories. These findings show that inter-laboratory reproducibility of IRIF-based biodosimetry depends primarily on workflow harmonization rather than on pharmacological modulation of DNA damage signaling.

Analysis of freshly isolated PBL served as a within-laboratory control to assess whether conclusions derived from cryopreserved UCBL were workflow-dependent. PBL showed consistent dose-dependent induction of all IRIF endpoints, with foci yields at 100 mGy exceeding those observed in UCBL from Laboratory 1 and closely matching UCBL data from Laboratory 2. Importantly, γH2AX pan-staining was absent in PBL under all experimental conditions, underscoring system-dependent differences between UCBL and PBL under the examined conditions and minimizing apoptosis-related confounding in fresh cells. At the highest dose tested (1000 mGy), cal A treatment in PBL was associated with a reduction in γH2AX/53BP1 co-localized foci relative to DMSO controls, a pattern consistent with altered repair kinetics or apoptosis-related chromatin changes rather than foci stabilization. Under the tested low-dose, early post-irradiation conditions, this study rules out cal A as a generally applicable strategy for improving IRIF-based biodosimetric robustness.

4.2 Positioning Within the Literature

Phosphatase inhibition by cal A has been reported to affect γH2AX signaling in several experimental systems, although with substantial context dependence [32,34]. In adult PBL, Kuefner *et al*. (2013) [31] reported prolonged γH2AX foci persistence after low-dose irradiation in the presence of cal A, while effects on 53BP1 were limited. Importantly, these experiments differed from the present study in post-irradiation timing, workflow structure, and analytical endpoints. By contrast, under harmonized low-dose workflows optimized for early biodosimetric readout, the present study did not detect a consistent stabilizing effect of calyculin A on γH2AX or 53BP1 foci. These discrepancies are more plausibly explained by differences in workflow design, post-irradiation timing, dose range, and analytical thresholds than by cal A efficacy *per se*. Recent reviews emphasize that such context dependency is a central challenge in biodosimetry assay standardization [17,42].

The PBL dataset was included to test the internal consistency of conclusions under conditions free of cryopreservation-related stress. While UCBL showed no cal A effect across the examined dose range, PBL displayed a reduction in γH2AX/53BP1 co-localization at high dose under cal A treatment. This observation supports the notion that cal A's impact depends not only on timing and workflow but also on intrinsic biological properties of the cell system. The results do not contradict earlier reports of cal A effects, but delimit their applicability: under rapid, harmonized low-dose biodosimetry workflows, pharmacological phosphatase inhibition does not improve assay robustness.

Comparison With Our Previous Study

The present findings directly extend and reinforce our earlier observations in UCBL [36]. In that study, γH2AX, 53BP1, and co-localized foci exhibited highly linear dose-response relationships, with co-localization representing the most sensitive endpoint. The current inter-laboratory design reproduces these patterns and further demonstrates that sensitivity and linearity are preserved across laboratories and fixation times.

Inclusion of freshly isolated PBL adds an important dimension, indicating that donor variability, fixation timing, and cryopreservation stress contribute to absolute yield differences [43–45].

Across both studies, DMSO was confirmed as a neutral vehicle control, and cal A at 1 nM consistently failed to stabilize IRIF. Higher concentrations previously shown to induce cytotoxicity and apoptosis [36] were deliberately excluded from the present comparison. Together, these datasets converge on a coherent interpretation in which low, non-toxic concentrations of cal A do not measurably enhance IRIF stability, whereas higher concentrations trigger apoptosis-related chromatin alterations that confound biodosimetric readouts.

4.3 Inter-laboratory Variability and Methodological Robustness

Systematic offsets in absolute IRIF yields between laboratories are a well-recognized feature of multicenter biodosimetry studies and do not, by themselves, indicate methodological failure [15,17,46]. In the present study, such offsets did not alter dose-response linearity or qualitative treatment conclusions. These findings are directly relevant to ongoing biodosimetry standardization efforts within international networks such as RENEB and EURADOS, which increasingly prioritize workflow harmonization over absolute inter-laboratory yield matching. Accordingly, the objective of inter-laboratory comparison in this study was not to eliminate absolute yield differences, but to determine whether harmonized workflows preserve interpretable and reproducible dose-response behavior. Recent methodological analyses converge on the same conclusion: reproducibility in IRIF-based biodosimetry is achieved through disciplined workflow alignment rather than through incremental assay sensitivity gains [47,48].

4.4 Biological Interpretation and Implications

Consistent correlations among γH2AX, 53BP1, and co-localized foci support co-localization as the most robust readout for low-dose DSB detection under harmonized assay conditions. By contrast, γH2AX pan-nuclear staining did not track with IRIF-based endpoints and should be interpreted separately from repair-associated foci under low-dose conditions [16,26,27,37,38]. This distinction is particularly relevant when evaluating cal A, as phosphatase inhibition can alter chromatin-associated signaling without improving repair foci-based readouts.

Standardized IRIF assays without pharmacological modifiers provide reliable and interpretable dose-response information in the low-dose range relevant for biodosimetry [2,6,49,50]. While cal A remains useful in specific radiobiological applications, such as premature chromosome condensation assays [51–54], its routine use as an enhancer of IRIF-based biodosimetry is not supported under harmonized low-dose workflows.

Future work should focus on validating IRIF-based biodosimetry under realistic operational constraints, including delayed processing and inter-operator variability, rather than on pharmacological signal amplification [55]. From a translational perspective, these findings argue for abandoning cal A as a default 'fix' for inter-laboratory variability and instead prioritizing disciplined workflow harmonization.

5. Conclusions

This study provides an inter-laboratory evaluation of γH2AX/53BP1-based IRIF responses of human normal G_0 lymphocytes to low-dose IR under harmonized low-dose biodosimetry workflows. By integrating analyses of cryopreserved UCBL and freshly isolated PBL, the study sep-

arates workflow-dependent effects from biologically interpretable IRIF responses.

Our results demonstrate that γH2AX, 53BP1, and colocalized foci exhibit robust, linear dose-response relationships across both systems, while γH2AX pan-staining represents a distinct apoptosis-associated endpoint. At a non-toxic concentration of 1 nM, cal A does not provide a consistent benefit for IRIF-based biodosimetry under the tested low-dose conditions. Under higher-dose conditions, phosphatase inhibition altered IRIF patterns without improving interpretability for biodosimetric purposes.

Collectively, these findings indicate that cal A should not be regarded as a default enhancer of γH2AX/53BP1-based biodosimetry. Instead, its effects are context-dependent, influenced by cell type, irradiation dose, and pre-analytical workflow. Under harmonized and timely laboratory conditions, cal A offers no measurable advantage at non-toxic concentrations.

By demonstrating reproducibility across laboratories and biological systems, this work strengthens confidence in IRIF-based biodosimetry as a standardized and translatable tool. These results further support integration of IRIF-based biodosimetry into automated and predictive scoring platforms for radiation preparedness and clinical triage. Recent integrative analyses further underscore that such progress toward automation and predictive biodosimetry critically depends on rigorously validated, reproducible experimental foundations rather than on incremental assay sensitivity gains alone. Instead, reproducibility of IRIF-based biodosimetry is best achieved through disciplined workflow harmonization rather than through pharmacological intervention.

Availability of Data and Materials

The datasets used or analyzed during the current study are available from the corresponding author on reasonable request.

Author Contributions

Conceptualization, LZ, LJ; methodology, LZ, LJ; software, LZ; validation, JK, PP; formal analysis, LZ, JK, PP and LJ; investigation, LZ, LJ and JK; resources, LZ; data curation, LZ, JK and LJ; writing-original draft preparation, LZ and LJ; writing-review and editing, LZ; visualization, LZ and LJ; supervision, LZ; project administration, LZ; funding acquisition, LZ. All authors contributed to editorial changes in the manuscript. All authors read and approved the final manuscript. All authors have participated sufficiently in the work and agreed to be accountable for all aspects of the work.

Ethics Approval and Consent to Participate

The study was conducted in accordance with the ethical principles outlined in the Declaration of Helsinki. UCB samples were obtained from Eurocord-Slovakia, a non-profit public umbilical cord blood bank. According to Slovak national regulations, the use of fully anonymized biological material provided by a public tissue bank for research purposes does not require additional ethical committee approval. Donor recruitment and primary UCB sample collection were conducted in accordance with national regulations and institutional ethical guidelines. PBL donor recruitment and participation were supervised by the local Ethics Committee of the Biomedical Research Center, Slovak Academy of Sciences, Bratislava, Slovakia (approval No. EK/BmV-01/2023). The local ethical protocols required that all PBL donors or their legal guardians provided informed consent prior to blood sample collection.

Acknowledgment

The authors would like to thank M. Kubes, Eurocord-Slovakia, Bratislava, Slovakia, for providing UCB MNC; V. Vinnikov, PhD. and I. Belyaev, Assoc. Prof., D.Sc., Department of Radiobiology, Cancer Research Institute, Biomedical Research Center, Slovak Academy of Sciences, Bratislava, Slovakia, for consulting on statistical issues of the study; E. Hajtmanova, M.D. and Z. Zaborska, Oncology Centre of Jessenius Faculty of Medicine in Martin, Comenius University in Bratislava and Martin University Hospital, Martin, Slovakia, and G. Kralik and K. Kontrisova, St. Elisabeth Cancer Institute, Bratislava, Slovakia for assistance and *in vitro* irradiations of the cells.

Funding

This research was funded by the Recovery and Resilience Plan of the Slovakia under the project [CU-ESG-2024-05-PD] - administered by the Research Agency under the Grant Agreement No. 09I03-03-V05-00019 and by the Grant Agency of the Slovakia (VEGA) under Grant [2/0140/23].

Conflict of Interest

The authors declare no conflict of interest. The funders had no role in the design of the study; in the collection, analyses, or interpretation of data; in the writing of the manuscript, or in the decision to publish the results.

Supplementary Material

Supplementary material associated with this article can be found, in the online version, at https://doi.org/10.31083/FBL47070.

References

[1] Escalona MB, Ryan TL, Balajee AS. Current developments in biodosimetry tools for radiological/nuclear mass casualty incidents. Environmental Advances. 2022; 9: 100265. https://doi.org/10.1016/j.envadv.2022.100265.

[2] Widjaja L, Werner RA, Krischke E, Christiansen H, Bengel FM, Bogdanova N, *et al*. Individual radiosensitivity reflected by γ-H2AX and 53BP1 foci predicts outcome in PSMA-targeted radioligand therapy. European Journal of Nuclear Medicine

and Molecular Imaging. 2023; 50: 602–612. https://doi.org/10.1007/s00259-022-05974-8.

[3] Imano N, Nishibuchi I, Kawabata E, Kinugasa Y, Shi L, Sakai C, *et al*. Evaluating Individual Radiosensitivity for the Prediction of Acute Toxicities of Chemoradiotherapy in Esophageal Cancer Patients. Radiation Research. 2020; 195: 244–252. https://doi.org/10.1667/RADE-20-00234.1.

[4] Ignatov MA, Chigasova AK, Osipov AA, Fedotov YA, Vorobyeva NY, Osipov AN. Effect of X-Ray Energy on the Quantitative Yield of γH2AX and 53BP1 Foci in Human Mesenchymal Stem Cells. Bulletin of Experimental Biology and Medicine. 2025; 178: 717–721. https://doi.org/10.1007/s10517-025-06404-z.

[5] Osipov A, Chigasova A, Yashkina E, Ignatov M, Vorobyeva N, Zyuzikov N, *et al*. Early and Late Effects of Low-Dose X-ray Exposure in Human Fibroblasts: DNA Repair Foci, Proliferation, Autophagy, and Senescence. International Journal of Molecular Sciences. 2024; 25: 8253. https://doi.org/10.3390/ijms25158253.

[6] Bogdanova NV, Jguburia N, Ramachandran D, Nischik N, Stemwedel K, Stamm G, *et al*. Persistent DNA Double-Strand Breaks After Repeated Diagnostic CT Scans in Breast Epithelial Cells and Lymphocytes. Frontiers in Oncology. 2021; 11: 634389. https://doi.org/10.3389/fonc.2021.634389.

[7] Lacko A, Madarasz S, Kolejak K, Babecka J, Lackova L. Parkinson's Disease Diagnosis with I Ioflupane (DaTSCAN). American Journal of Internal Medicine. 2024; 12: 40–55. https://doi.org/10.11648/j.ajim.20241204.11.

[8] Schumann S, Eberlein U, Lapa C, Müller J, Serfling S, Lassmann M, *et al*. α-Particle-induced DNA damage tracks in peripheral blood mononuclear cells of [223Ra]RaCl2-treated prostate cancer patients. European Journal of Nuclear Medicine and Molecular Imaging. 2021; 48: 2761–2770. https://doi.org/10.1007/s00259-020-05170-6.

[9] Lacko A, Straka J, Hrubon A, Babecka J, Lacko L. Myocardial Perfusion Scintigraphy in Diagnosics of Coronary Heart Disease. American Journal of Internal Medicine. 2024; 12: 63–73. https://doi.org/10.11648/j.ajim.20241205.11.

[10] Lacko L, Babecka J. Analysis of Safety Aspects in Nuclear Medicine in the Comparison of Cardio Cameras. CSWHI. 2023; 14: 53–60. https://doi.org/10.22359/cswhi_14_4_08.

[11] Vinnikov V, Belyakov O. CLINICAL APPLICATIONS OF BIOMARKERS OF RADIATION EXPOSURE: LIMITATIONS AND POSSIBLE SOLUTIONS THROUGH COORDINATED RESEARCH. Radiation Protection Dosimetry. 2019; 186: 3–8. https://doi.org/10.1093/rpd/ncz038.

[12] Vinnikov VA, Belyakov O. Radiation Exposure Biomarkers in the Practice of Medical Radiology: Cooperative Research and the Role of the International Atomic Energy Agency (IAEA) Biodosimetry/Radiobiology Laboratory. Health Physics. 2020; 119: 83–94. https://doi.org/10.1097/HP.0000000000001266.

[13] Vinnikov V, Hande MP, Wilkins R, Wojcik A, Zubizarreta E, Belyakov O. Prediction of the Acute or Late Radiation Toxicity Effects in Radiotherapy Patients Using Ex Vivo Induced Biodosimetric Markers: A Review. Journal of Personalized Medicine. 2020; 10: 285. https://doi.org/10.3390/jpm10040285.

[14] O'Brien G, Cruz-Garcia L, Majewski M, Grepl J, Abend M, Port M, *et al*. FDXR is a biomarker of radiation exposure in vivo. Scientific Reports. 2018; 8: 684. https://doi.org/10.1038/s41598-017-19043-w.

[15] Belyaev IY. Radiation-induced DNA repair foci: spatio-temporal aspects of formation, application for assessment of radiosensitivity and biological dosimetry. Mutation Research. 2010; 704: 132–141. https://doi.org/10.1016/j.mrrev.2010.01.011.

[16] Durdik M, Kosik P, Gursky J, Vokalova L, Markova E, Belyaev I. Imaging flow cytometry as a sensitive tool to detect low-dose-induced DNA damage by analyzing 53BP1 and γH2AX foci in human lymphocytes. Cytometry. Part a: the Journal of the International Society for Analytical Cytology. 2015; 87: 1070–1078. https://doi.org/10.1002/cyto.a.22731.

[17] Valente D, Gentileschi MP, Guerrisi A, Bruzzaniti V, Morrone A, Soddu S, *et al*. Factors to Consider for the Correct Use of γH2AX in the Evaluation of DNA Double-Strand Breaks Damage Caused by Ionizing Radiation. Cancers. 2022; 14: 6204. https://doi.org/10.3390/cancers14246204.

[18] Prabhu KS, Kuttikrishnan S, Ahmad N, Habeeba U, Mariyam Z, Suleman M, *et al*. H2AX: A key player in DNA damage response and a promising target for cancer therapy. Biomedicine & Pharmacotherapy = Biomedecine & Pharmacotherapie. 2024; 175: 116663. https://doi.org/10.1016/j.biopha.2024.116663.

[19] Jakl L, Marková E, Kolářiková L, Belyaev I. Biodosimetry of Low Dose Ionizing Radiation Using DNA Repair Foci in Human Lymphocytes. Genes. 2020; 11: 58. https://doi.org/10.3390/genes11010058.

[20] Chaurasia RK, Shirsath KB, Desai UN, Bhat NN, Sapra BK. Establishment of *in vitro* Calibration Curve for ^{60}Co-γ-rays Induced Phospho-53BP1 Foci, Rapid Biodosimetry and Initial Triage, and Comparative Evaluations With γH2AX and Cytogenetic Assays. Frontiers in Public Health. 2022; 10: 845200. https://doi.org/10.3389/fpubh.2022.845200.

[21] Redon CE, Nakamura AJ, Gouliaeva K, Rahman A, Blakely WF, Bonner WM. The use of gamma-H2AX as a biodosimeter for total-body radiation exposure in non-human primates. PloS One. 2010; 5: e15544. https://doi.org/10.1371/journal.pone.0015544.

[22] Rahman MZ, Islam S, Kamal AHM, Rana AYKMM, Roy PK. Advancement in Biodosimetry Techniques and Their Growing Role in Nuclear Medicine. Journal of Biosciences and Medicines. 2025; 13: 1–24. https://doi.org/10.4236/jbm.2025.137001.

[23] Kosik P, Durdik M, Jakl L, Skorvaga M, Markova E, Vesela G, *et al*. DNA damage response and preleukemic fusion genes induced by ionizing radiation in umbilical cord blood hematopoietic stem cells. Scientific Reports. 2020; 10: 13722. https://doi.org/10.1038/s41598-020-70657-z.

[24] Vinnikov V, Belyakov O. Clinical Applications of Biological Dosimetry in Patients Exposed to Low Dose Radiation Due to Radiological, Imaging or Nuclear Medicine Procedures. Seminars in Nuclear Medicine. 2022; 52: 114–139. https://doi.org/10.1053/j.semnuclmed.2021.11.008.

[25] Jakl L, Lobachevsky P, Vokálová L, Durdík M, Marková E, Belyaev I. Validation of JCountPro software for efficient assessment of ionizing radiation-induced foci in human lymphocytes. International Journal of Radiation Biology. 2016; 92: 766–773. https://doi.org/10.1080/09553002.2016.1222093.

[26] Durdik M, Kosik P, Kruzliakova J, Jakl L, Markova E, Belyaev I. Hematopoietic stem/progenitor cells are less prone to undergo apoptosis than lymphocytes despite similar DNA damage response. Oncotarget. 2017; 8: 48846–48853. https://doi.org/10.18632/oncotarget.16455.

[27] Vasilyev SA, Kubes M, Markova E, Belyaev I. DNA damage response in CD133 + stem/progenitor cells from umbilical cord blood: low level of endogenous foci and high recruitment of 53BP1. International Journal of Radiation Biology. 2013; 89: 301–309. https://doi.org/10.3109/09553002.2013.754555.

[28] Nayak AA, Mumbrekar KD, Rao BSS. Pharmacological approach to increasing the retention of radiation-induced γ-H2AX foci using phosphatase inhibitors: significance in radiation biodosimetry. Journal of Radiological Protection: Official Journal of the Society for Radiological Protection. 2018; 38: 318–328. https://doi.org/10.1088/1361-6498/aaa97a.

[29] Honkanen RE, Golden T. Regulators of serine/threonine protein phosphatases at the dawn of a clinical era? Current Medicinal Chemistry. 2002; 9: 2055–2075. https://doi.org/10.2174/0929867023368836.

[30] Chowdhury D, Keogh MC, Ishii H, Peterson CL, Buratowski S, Lieberman J. gamma-H2AX dephosphorylation by protein phosphatase 2A facilitates DNA double-strand break repair. Molecular Cell. 2005; 20: 801–809. https://doi.org/10.1016/j.molcel.2005.10.003.

[31] Kuefner MA, Brand M, Engert C, Kappey H, Uder M, Distel LV. The effect of calyculin A on the dephosphorylation of the histone γ-H2AX after formation of X-ray-induced DNA double-strand breaks in human blood lymphocytes. International Journal of Radiation Biology. 2013; 89: 424–432. https://doi.org/10.3109/09553002.2013.767991.

[32] Nazarov IB, Smirnova AN, Krutilina RI, Svetlova MP, Solovjeva LV, Nikiforov AA, *et al*. Dephosphorylation of histone gamma-H2AX during repair of DNA double-strand breaks in mammalian cells and its inhibition by calyculin A. Radiation Research. 2003; 160: 309–317. https://doi.org/10.1667/rr3043.

[33] Kanda R, Eguchi-Kasai K, Hayata I. Phosphatase inhibitors and premature chromosome condensation in human peripheral lymphocytes at different cell-cycle phases. Somatic Cell and Molecular Genetics. 1999; 25: 1–8. https://doi.org/10.1023/b:scam.0000007135.12486.e3.

[34] Antonelli F, Belli M, Cuttone G, Dini V, Esposito G, Simone G, *et al*. Induction and repair of DNA double-strand breaks in human cells: dephosphorylation of histone H2AX and its inhibition by calyculin A. Radiation Research. 2005; 164: 514–517. https://doi.org/10.1667/rr3379.1.

[35] Roch-Lefèvre S, Mandina T, Voisin P, Gaëtan G, Mesa JEG, Valente M, *et al*. Quantification of gamma-H2AX foci in human lymphocytes: a method for biological dosimetry after ionizing radiation exposure. Radiation Research. 2010; 174: 185–194. https://doi.org/10.1667/RR1775.1.

[36] Zastko L, Račková A, Petrovičová P, Durdík M, Míšek J, Marková E, *et al*. Evaluation of Calyculin A Effect on γH2AX/53BP1 Focus Formation and Apoptosis in Human Umbilical Cord Blood Lymphocytes. International Journal of Molecular Sciences. 2021; 22: 5470. https://doi.org/10.3390/ijms22115470.

[37] Solier S, Pommier Y. The apoptotic ring: a novel entity with phosphorylated histones H2AX and H2B and activated DNA damage response kinases. Cell Cycle (Georgetown, Tex.). 2009; 8: 1853–1859. https://doi.org/10.4161/cc.8.12.8865.

[38] Anglada T, Terradas M, Hernández L, Genescà A, Martín M. Analysis of Residual DSBs in Ataxia-Telangiectasia Lymphoblast Cells Initiating Apoptosis. BioMed Research International. 2016; 2016: 8279560. https://doi.org/10.1155/2016/8279560.

[39] Marková E, Somsedíková A, Vasilyev S, Pobijaková M, Lacková A, Lukačko P, *et al*. DNA repair foci and late apoptosis/necrosis in peripheral blood lymphocytes of breast cancer patients undergoing radiotherapy. International Journal of Radiation Biology. 2015; 91: 934–945. https://doi.org/10.3109/09553002.2015.1101498.

[40] Zastko L, Bereta M, Timko J, Belyaev I. Classifier Spot Count Optimization of Automated Fluorescent Slide Scanning System. Acta Medica Martiniana. 2022; 22: 24–33. https://doi.org/10.2478/acm-2022-0004.

[41] Ainsbury EA, Lloyd DC. Dose estimation software for radiation biodosimetry. Health Physics. 2010; 98: 290–295. https://doi.org/10.1097/01.HP.0000346305.84577.b4.

[42] Felgentreff K, Schuetz C, Baumann U, Klemann C, Viemann D, Ursu S, *et al*. Differential DNA Damage Response of Peripheral Blood Lymphocyte Populations. Frontiers in Immunology. 2021; 12: 739675. https://doi.org/10.3389/fimmu.2021.739675.

[43] Bankoglu EE, Stipp F, Gerber J, Seyfried F, Heidland A, Bahner U, *et al*. Effect of cryopreservation on DNA damage and DNA repair activity in human blood samples in the comet assay. Archives of Toxicology. 2021; 95: 1831–1841. https://doi.org/10.1007/s00204-021-03012-4.

[44] Marino M, Gigliotti L, Møller P, Riso P, Porrini M, Del Bo C. Impact of 12-month cryopreservation on endogenous DNA damage in whole blood and isolated mononuclear cells evaluated by the comet assay. Scientific Reports. 2021; 11: 363. https://doi.org/10.1038/s41598-020-79670-8.

[45] Vigašová K, Durdík M, Jakl L, Dolinská Z, Pobijaková M, Fekete M, *et al*. Chemotherapy and cryopreservation affects DNA repair foci in lymphocytes of breast cancer patients. International Journal of Radiation Biology. 2023; 99: 1660–1668. https://doi.org/10.1080/09553002.2023.2211140.

[46] Sekikawa Y, Kato TA. Radiation-Induced Gamma-H2AX Foci Staining and Analysis. Methods in Molecular Biology (Clifton, N.J.). 2025; 2933: 25–29. https://doi.org/10.1007/978-1-0716-4574-1_4.

[47] Bolcaen J, Combrink N, Spoormans K, More S, Vandevoorde C, Fisher R, *et al*. Biodosimetry, can it find its way to the nuclear medicine clinic? Frontiers in Nuclear Medicine. 2023; 3: 1209823. https://doi.org/10.3389/fnume.2023.1209823.

[48] Granzotto A, El Nachef L, Restier-Verlet J, Sonzogni L, Al-Choboq J, Bourguignon M, *et al*. When Chromatin Decondensation Affects Nuclear γH2AX Foci Pattern and Kinetics and Biases the Assessment of DNA Double-Strand Breaks by Immunofluorescence. Biomolecules. 2024; 14: 703. https://doi.org/10.3390/biom14060703.

[49] Derlin T, Bogdanova N, Ohlendorf F, Ramachandran D, Werner RA, Ross TL, *et al*. Assessment of γ-H2AX and 53BP1 Foci in Peripheral Blood Lymphocytes to Predict Subclinical Hematotoxicity and Response in Somatostatin Receptor-Targeted Radionuclide Therapy for Advanced Gastroenteropancreatic Neuroendocrine Tumors. Cancers. 2021; 13: 1516. https://doi.org/10.3390/cancers13071516.

[50] Shi L, Tashiro S. Estimation of the effects of medical diagnostic radiation exposure based on DNA damage. Journal of Radiation Research. 2018; 59: ii121–ii129. https://doi.org/10.1093/jrr/rry006.

[51] Sun M, Moquet J, Lloyd D, Ainsbury E. A faster and easier biodosimetry method based on calyculin A-induced premature chromosome condensation (PCC) by scoring excess objects. Journal of Radiological Protection: Official Journal of the Society for Radiological Protection. 2020; 40: 892–905. https://doi.org/10.1088/1361-6498/aba085.

[52] Puig R, Pujol M, Barrios L, Caballín MR, Barquinero JF. Analysis of α-particle-induced chromosomal aberrations by chemically-induced PCC. Elaboration of dose-effect curves. International Journal of Radiation Biology. 2016; 92: 493–501. https://doi.org/10.1080/09553002.2016.1206238.

[53] Smith TL, Ryan TL, Escalona MB, Shuryak IE, Balajee AS. Application of FISH based G2-PCC assay for the cytogenetic assessment of high radiation dose exposures: Potential implications for rapid triage biodosimetry. PloS One. 2024; 19: e0312564. https://doi.org/10.1371/journal.pone.0312564.

[54] Rawojć K, Miszczyk J, Możdżeń A, Swakoń J, Sowa-Staszczak A. Evaluation of the premature chromosome condensation scoring protocol after proton and X-ray irradiation of human peripheral blood lymphocytes at high doses range. International Journal of Radiation Biology. 2018; 94: 996–1005. https://doi.org/10.1080/09553002.2018.1490038.

[55] Młynarczyk D, Puig P, Armero C, Gómez-Rubio V, Barquinero JF, Pujol-Canadell M. Radiation dose estimation with time-since-exposure uncertainty using the [Formula: see text]-H2AX biomarker. Scientific Reports. 2022; 12: 19877. https://doi.org/10.1038/s41598-022-24331-1.